Article

Preparation of Silicon Oxycarbide (SiCO) Ceramics from Different Polymer Architectures and Assessment on the Performance as Electrodic Materials for Voltammetric Sensing of Antioxidant Phenolic Compounds

Lívia R. C. Silva,[a] Maria A. Silva,[a] Paulo Rogério C. da Silva,[b]
César Ricardo T. Tarley *,[a] and Mariana G. Segatelli[a]

[a]Departamento de Química, Universidade Estadual de Londrina,
Celso Garcia Cid, PR 445, km 380, CP 10.011, Londrina-PR, Brazil

[b]Departamento de Física, Universidade Estadual de Londrina,
Celso Garcia Cid, PR 445, km 380, CP 10.011, Londrina-PR, Brazil

Silicon oxycarbide (SiCO) ceramics obtained from polymer pyrolysis and with varied carbon contents were prepared and evaluated as new electrodic materials for sensing of *tert*-butylhydroquinone (TBHQ) and butylated hydroxyanisole (BHA) antioxidants. Three polymers were synthesized varying molecular architecture and aromatic carbon groups, followed by pyrolysis at 1000 and 1500 °C to obtain SiCO ceramics. Graphitization and crystallization processes were evidenced, in different extent, according to precursor chemistry. SiCO at 1500 °C with intermediary carbon content provided slight improvement in the peak anodic separation of TBHQ and BHA and higher peak current compared with glassy carbon electrode (GCE). Higher acidic sites concentration together with more ordered residual carbon phase produced *in situ* contributed to great electrochemical performance of SiCO towards phenolic compounds detection. Therefore, the ceramic herein prepared exhibits highly efficient features as a new SiCO composited electrode for simultaneous determination of antioxidant phenolic compounds bearing in mind further analytical applications.

Keywords: polymer, carbon content, pyrolysis, ceramic, sensors

Introduction

Development of silicon oxycarbide (SiCO)-based materials in polymer derived ceramics (PDC) field has gained great interest of researchers, due to their desirable mechanical, optical and electrical properties, together with high chemical and oxidation resistances and low densities.[1] These properties allow their use in several technological applications including anodes for lithium ion batteries,[2] electrochemical sensors,[3] biomedical components,[4] automotive parts,[5] catalyst support,[6] among others.

SiCO materials are usually obtained by controlled pyrolysis of poly(organosiloxanes) or their derivatives, under inert atmosphere. The fabrication process comprises the synthesis of preceramic silicon polymers, followed by the molding and/or curing and pyrolysis steps. Important structural transformations take place with the temperature increasing, basically involving organic-inorganic transition between 400 and 800 °C, development of amorphous ceramic network in the 800-1000 °C range and crystallization step at 1200-1600 °C.[7] Usually, the crystallization process occurs by phase separation (equation 1), in which SiCO decomposes into silicon carbide (SiC), silica (SiO_2) and C domains, as well as by carboreduction reaction (equation 2). In the latter process, silica is reduced by residual carbon, giving rise to SiC phase and CO releasing.[8]

$$2SiCO_{(s)} \rightarrow SiC_{(s)} + SiO_{2(s)} + C_{(s)} \qquad (1)$$
$$SiO_{2(s)} + 3C_{(s)} \rightarrow SiC_{(s)} + 2CO_{(g)} \qquad (2)$$
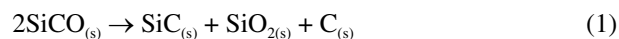
Overall, SiCO or SiC_xO_{4-x} ($0 \leq x \leq 4$) exhibits a mixed network composed of SiC_4, SiC_3O, SiC_2O_2, $SiCO_3$ and SiO_4 sites and residual carbon, besides the crystalline phases aforementioned, whose proportions depend on preceramic polymer chemistry and pyrolysis conditions.[9] Therefore, SiCO materials with complex microstructures can be

achieved from a careful choice of synthesis parameters. Due to versatility of the polymer pyrolysis route, many compounds might be incorporated in the polymeric network to modify structure and composition of ceramic products, thus amplifying their applications range.[10]

Carbon-rich SiCO materials can be satisfactorily fabricated from previous immobilization of carbonaceous compounds to poly(organosiloxanes), as a physically disperse phase,[11] or covalently bonded[3,12] at polymeric network structure. This last experimental strategy might be achieved by polymerization reactions well established in literature,[13-15] which are employed according to reactive functional groups at Si-polymers. Such approach favors the *in situ* production of residual carbon (or free carbon, C_{free}) through the incomplete degradation of organic groups at precursor structure. Polymers containing unsaturated organic groups usually give rise to higher C_{free} amounts regarding saturated organic groups, resulting in ceramics with higher electrical conductivities due to turbostratic carbon network formation at high temperatures.[16] Since C_{free} phase is composed of Csp^2 and Csp^3 sites whose amounts and distributions vary as a function of both precursors and pyrolysis conditions, electrical characteristics might be tuned to fabricate materials with electrochemical potentialities. As described earlier, the presence of C_{free} phase plays an important role to induce SiC crystallization via carboreduction reaction (equation 2) through its consumption with SiO_2 sites, intensifying the development of electrically active phases.[7,10]

SiCO ceramics and ceramic composites containing activated charcoal have already been shown good electrochemical response for acetaminophen, as reported by our research group.[3] The presence of the extra carbonaceous phase together with hybrid polymeric precursors composition played a great role on oxidation of acetaminophen due to production of multi-walled carbon nanotubes (MWCNT) and SiC in different extent into ceramic matrix. Although the effect of additional carbon phase to Si-precursors on electrochemical response of SiCO-based ceramics has been described,[3] a comparative study involving different polymer architectures on phases development for this purpose has not been exploit yet. In this sense, C_{free} phase exclusively produced into SiCO matrices from degradation of additive-free polymer precursors combined with its influence on development of SiC via carboreduction reaction (equation 2) is a promising approach for fabrication of Si-polymers derived ceramics with potentialities to be employed as electrodic material for sensing synthetic phenolic antioxidants (SPA) compounds. In the food industry, *tert*-butylhydroquinone (TBHQ) and hydroxyanisole (BHA) have been the most

used for protecting lipid food against detrimental change of oxidizable nutrients.[17] Although several analytical methods based on high-performance liquid chromatography, UV-visible spectrophotometry and gas chromatography have been widely used for detecting SPA, the electrochemical devices provide low instrumentation cost, rapid analysis and easy operation.[18] However, the performance of electrochemical sensors in terms of sensitivity, selectivity and anti-fouling properties, depends on composition/nature of electrodic material.

According to aforementioned, the aim of the present article was to synthesize three preceramic polymers by varying the molecular architecture and carbon content, from different polymerization reactions, to obtain SiCO-based materials at 1000 and 1500 °C by pyrolysis route. Ceramic samples were further evaluated as electrodic materials for simultaneous determination of *tert*-butyl-hydroquinone (TBHQ) and butylated hydroxyanisole (BHA) antioxidants by cyclic voltammetry.

Experimental

Starting reagents

Silicones employed for synthesizing the preceramic polymers were poly(dimethylsiloxane-*co*-diphenylsiloxane) dihydroxy terminated (PDMF–OH), {HO–Si$(C_6H_5)_2$O[Si$(CH_3)_2$O]$_m$–[Si$(C_6H_5)_2$O]$_n$–Si$(C_6H_5)_2$–OH}, viscosity of ca. 60 cSt(lit.) or ca. 6×10^{-5} m^2 s^{-1} (25 °C), density of 1.05 g mL^{-1} and CAS No. 68951-93-9, 1,3,5,7-tetramethyl-1,3,5,7-tetravinylcyclotetrasiloxane (D$_4$Vi), [–Si(CH_3)(CH=CH$_2$)O–]$_4$, molar mass of 344.66 g mol^{-1}, density of 0.997 g mL^{-1} and CAS No. 2554-06-5, and poly(methylhydrosiloxane) (PMHS), [HSi(CH_3)O]$_n$, molar mass ca. 2450 g mol^{-1}, density of 1.006 g mL^{-1} and CAS No. 63148-57-2. Bisphenol A (BPA) (99%), molar mass of 228.29 g mol^{-1}, density of 1.200 g mL^{-1} and CAS No. 80-05-07, as well as divinylbenzene (DVB) (80%), molar mass of 130.19 g mol^{-1}, density of 0.914 g mL^{-1} and CAS No. 1321-74-0, were used as organic crosslinkers of the silicone chains. Dibutyltin diacetate (DDSn) $(CH_3CH_2CH_2CH_2)_2$Sn$(OCOCH_3)_2$, molar mass of 351.03 g mol^{-1}, density of 1.32 g mL^{-1} and CAS No. 1067-33-0, dicumyl peroxide [bis(1-methyl-1-phenylethyl)peroxide] (PDCM) (98%), molar mass of 270.37 g mol^{-1} and CAS No. 80-43-3, and a solution of 1,3-divinyl-1,1,3,3-tretramethyldisiloxane platinum(0) in poly(dimethylsiloxane) vinyl terminated, O[Si$(CH_3)_2$CH=CH$_2$]$_2$Pt, molar mass of 381.48 g mol^{-1}, density of 0.980 g mL^{-1} and CAS No. 68478-92-2, were employed as catalysts of polycondensation, radical and

hydrosilylation reactions, respectively. All reagents were acquired from Sigma-Aldrich (São Paulo, Brazil) and used as received without any further purification.

Synthesis of SiCO preceramic polymers

Preceramic polymer 1 (P1)

Preceramic polymer 1, with higher carbon content, was prepared by polycondensation reaction between PDMF–OH and BPA, in a 1:1 molar ratio, due to the presence of reactive hydroxyl groups in both structures. For this task, PDMF–OH silicone, organic crosslinker and 5 wt.% of dibutyltin diacetate catalyst were submitted to magnetic stirring during 1 h, in a beaker at room temperature for homogenization. After that, the mixture was poured into a porcelain crucible and placed in a muffle oven at 250 °C during 4 h for crosslinking step,[19] giving rise to preceramic polymer P1, which revealed brown color and physical appearance like foam.

Preceramic polymer 2 (P2)

Preceramic polymer 2, with lower carbon content, was obtained by radical polymerization involving D_4Vi chains, due to the reactive vinyl groups at cyclic silicone structure. For this procedure, D_4Vi and 1 wt.% dicumyl peroxide catalyst were added in a beaker and magnetically stirred at room temperature for 1 h and then submitted to the crosslinking process at 380 °C during 5 h,[7] under argon atmosphere. The resulting material, with yellow color and glassy appearance, was named preceramic polymer P2.

Preceramic polymer 3

Preceramic polymer 3, with intermediary carbon content, was synthesized by hydrosilylation reaction between PMHS and DVB, in a 1:1 molar ratio, due to the presence of respective Si–H and $H_2C=CH_2$ functional groups at starting reagents structure, according to the procedure previously described in literature.[20] Basically, DVB organic crosslinker and platinum catalyst were stirred during ca. 20 min for homogenization at room temperature. The solution was then submitted to an ice bath and nitrogen gas environment, followed by the slow PMHS addition. The solution remained under magnetic stirring until the gel point was achieved, which was immediately poured into Teflon molds. The resulting material was cured at room temperature for 30 min and post-cured at 120 °C for 4 h, giving rise to preceramic polymer P3, with light pink color and highly rigid appearance. Figure S5 (Supplementary Information (SI) section) illustrates the photo of all preceramic polymers synthesized.

Preparation of SiCO ceramics

SiCO ceramics were obtained by controlled pyrolysis of preceramic polymers, under argon atmosphere, employing a high temperature furnace containing an adapted alumina tube (EDG10P-S, São Carlos, Brazil). The thermal treatment step involved heating and cooling rates of 5 °C min^{-1}, up to two final temperatures, as described:

Pyrolysis procedure at final 1000 °C temperature: heating from ca. 25 to 700 °C (isotherm of 30 min), followed by heating to 1000 °C (isotherm of 120 min) and then, cooling procedure to ca. 25° C. Samples obtained from this pyrolysis ramp were named C1_1000, C2_1000 and C3_1000, according to preceramic polymer.

Pyrolysis procedure at final 1500 °C temperature: heating from ca. 25 to 700 °C (isotherm of 30 min), heating to 1000 °C (isotherm of 60 min) and up to 1500 °C (isotherm of 120 min) and then, cooling process to ca. 25 °C. Analogously, samples obtained from this pyrolysis ramp were named C1_1500, C2_1500 and C3_1500.

Pyrolysis at 1000 and 1500 °C were chosen due to important structural transformation events occurred at these two temperatures, such as redistribution reactions between the silicon sites and initial formation of residual carbon phase, followed by the crystallization process and phase segregation in the ceramic matrix.

After pyrolysis, all ceramic materials were ground to a fine powder and sieved ≤ 106 μm (Bertel Industry Metallurgic Ltda, Caieiras, Brazil) to get better control of particles size before characterization.

Characterization techniques

Thermal stability of polymer precursors was evaluated on a thermogravimetric analyzer (PerkinElmer, TGA 4000, Tokyo, Japan), using a temperature range from 25 to 900 °C, at 10 °C min^{-1} and nitrogen flowing of 20 mL min^{-1}. Thermogravimetric measurements were conducted with ca. 9 mg of samples and the ceramic yield was obtained by residual mass percentage at final temperature of 900 °C.

Fourier transform infrared (FTIR) spectra of the preceramic polymers and SiCO-based ceramics were acquired on a Fourier transform infrared spectrometer (Bruker®, Vertex 70, Dresden, Germany) with a platinum attenuated total reflectance (ATR) accessory. All spectra were registered in the 4000-400 cm^{-1} range, with 16 scans and spectral resolution of 4 cm^{-1}.

X-ray diffraction (XRD) measurements were performed on an X-ray diffractometer (PANanalytical, X'Pert PRO MPD, Malvern Panalytical, Almelo, Netherlands), operating with Cu Kα radiation (λ = 1.54060 Å), in Bragg Brentano geometry. XRD patterns were collected between 5 and

75° (2θ), with 0.0263° step-size and a time-counting of 100.0 s, operating at 40 kV and 30 mA at room temperature. To avoid preferred orientations in the sample preparation process and homogenize data collection, the powdered samples were rotated cyclically during measurements with a period of 1.0 s. To identify the crystalline phases, their relative weights and the lattice parameters of each crystalline structure, Rietveld refinements were carried out on the diffraction patterns by using the X'Pert High Score Plus software. Two measurements were performed on each sample, one with the pristine ceramic and another with the ceramic mixed with aluminium oxide internal standard at 70:30 (m/m) proportion. The Rietveld method was applied to the samples containing the aluminium oxide internal standard to determine the percentage of crystalline SiC and amorphous phase. In addition to aluminium oxide, SiC, SiO_2 and Sn phases were also identified, which were refined under PDF 01-074_2307, PDF 96-900-6286 and PDF 01-086-2265, respectively. To facilitate the visualization of the diffractograms and to better observe the characteristic peaks of the samples, only XRD patterns of pristine ceramic materials will be presented.

The average crystallite size (t) for SiC phase was estimated by the Scherrer formula according to equation 3.

$$t = \frac{K\lambda}{\beta\cos\theta} \tag{3}$$

where t is assigned to the average crystallite size, λ is the radiation wavelength in nanometers (0.15406 nm), β is the width at half height of the diffraction peak in radians, θ corresponds to half of the 2θ angle and K is a constant that depends on the particle morphology and ranges from 0.89 to 1.39 rad. As the crystallites obtained in this study have no defined shape, we employed K = 1, which corresponds to an apparent average volume size regardless of specific morphology.[21]

Carbon and hydrogen contents were determined in an elemental analyzer (PerkinElmer, 2400CHNS, Waltham, USA). During analysis, the powdered materials were submitted to total combustion at 1050 °C under oxygen. The resulting gases were separated in a column and CO_2 content was detected and quantified by a thermal conductivity detector (PerkinElmer, Waltham, Massachusetts, USA). The silicon amount was determined using the analytical curve method, in which a solid mixture involving silicon carbide (silicon source) into graphite (matrix) was employed. The solids were mixed in a vortex-type stirrer and the analyses were performed on a spectrophotometer (Shimadzu Corp., EDX 720, Tokyo, Japan) equipped with an X-ray tube containing rhodium anode and Si(Li) detector cooled with liquid nitrogen. The analyses were conducted at 15 kV of voltage, 1000 mA of current, using a collimator of 3 mm and life time of 100 s. Analytical curve was constructed with nine points, in a range from 30 to 70% silicon (in mass), resulting in a SF = 0.0097%Si + 0.3 equation, where SF is the fluorescence signal and %Si is the percentage in mass of silicon, with correlation factor (r^2) of 1. Finally, the oxygen amount was estimated by difference among the carbon, hydrogen and silicon contents.

Empirical and stoichiometric formulae of the preceramic polymers and SiCO ceramics were obtained, according to Dibandjo *et al.*[22] The authors consider the value of each element adjusted to one mole of silicon, by means the ratio among the carbon or oxygen moles' number with the silicon moles. These values were applied to the general formula illustrated in equation 4 to obtain the values corresponding to carbon bounded to polymeric or ceramic networks as well as free carbon (C_{free}).[23]

$$SiC_xO_{2(1-x)} + yC_{free} \tag{4}$$

where x represents the proportion of Si–C bonds, (1-x) the proportion of Si–O bonds, considering the different SiO_2 and SiC stoichiometries from the charges balance of Si^{4+}, C^{4-} and O^{2-} species, and y represents the stoichiometry of C_{free} phase.

To assess the C_{free} phase produced into ceramic matrices, Raman spectroscopy analyses were performed on a confocal spectrometer (WITec, Alpha300+, Abingdon, United Kingdom), with a laser light at 532 nm for excitation and 8 cm^{-1} of resolution. Two measurements were made in different regions and the average spectrum was registered for each sample. All samples were measured in the powder form. Raman spectra were submitted to mathematical fitting employing Lorentzian function[24] to obtain more accurately parameters related to D and G bands. Lateral average carbon-domains size (La) was calculated in accordance with equation 5, proposed by Ferrari and Robertson,[24] suitable for systems containing disordered carbon domains.

$$\frac{I(D)}{I(G)} = C(\lambda)La^2 \tag{5}$$

where La is the lateral carbon-domain size, I(D) and I(G) are the intensities of respective D and G bands, the coefficient C depends on the wavelength of monochromatic radiation, and in this study is equal to 0.62 nm^{-2}, according to radiation of 532 nm.

The morphology of the preceramic polymers and ceramic materials was examined by scanning electron microscopy (SEM), using a scanning electron microscope

(FEI QUANTA 200, New York, USA), with a 25 keV accelerating voltage. The powdered samples were put on SEM standard grid and coated with a thin layer of gold (30 nm) prior to analyses, in a sputter coater equipment (Bal-Tec SCD, Pfäffikon, Switzerland), in order to minimize charging under the incident electron beam.

Static contact angle measurement

In order to evaluate the wettability of SiCO-based pastes, the static contact angles were investigated by the sessile drop method.[25] Onto the surface of electrodes prepared with C1, C2 and C3 ceramic materials, a water droplet of 20 μL was carefully deposited. The photographs were taken on a Samsung Galaxy S20 FE cell phone, equipped with a 12 MPX Samsung S5K2LD sensor, type Isocell, with a sensor 1/1.76 and a pixel size of 1.8 μm. Contact angles were measured with ImageJ® software.[26]

Boehm's titration procedure

Boehm titration was carried out to evaluate the total content of acidic sites in the ceramic materials. Such result together with wettability data might help an insight into the electrochemical behavior of the ceramic materials in voltammetric measures. The titration was performed by dispersing 0.5 g of each ceramic material (C1, C2, and C3) in 25.0 mL of standardized 0.1 mol L^{-1} NaOH and stirred for 24 h. After this time, the dispersion was filtered, and a 5.0 mL aliquot was titrated with standardized HCl. The acidic sites were quantified by the difference in the number of moles at the equivalence point of the NaOH solution before and after the stirring period.[27]

Electrochemical assay for *tert*-butylhydroquinone (TBHQ) and butylated hydroxyanisole (BHA) determination employing SiCO ceramics as electrodic materials

Electrochemical measurements were performed at room temperature, with a potentiostat/galvanostat PalmSens (Palm Instruments BV®, Houten, Netherlands), controlled by software Palm Instruments BV® PS Trace 5.8 (Houten, Netherlands). A conventional three-electrode electrochemical cell containing a reference electrode (Ag/AgCl, 3.0 mol L^{-1}), an auxiliary electrode (spiral platinum wire) and a working electrode (ceramic paste) were used. The working electrode was prepared by mixing 32.0 mg of SiCO ceramics with 8.0 mg of mineral oil (Nujol®), resulting in an 80:20 wt.% ratio, and homogenizing in a Petri dish with a stainless steel spatula until a uniform paste was obtained. The paste was carefully

inserted and compacted into a Teflon tube, with a cavity of 0.188 cm^2. The surface of the electrode was polished with paper flat surface and washed with ultrapure water. Cyclic voltammograms were acquired using TBHQ and BHA ethanol solution at 0.1 mmol L^{-1} concentration and BR buffer solution at 0.3 mol L^{-1} concentration (pH 2.0), employing scan rate of 50 mV s^{-1}. In order to compare the electrochemical behavior of SiOC ceramics as electrodic materials, a commercial glassy carbon electrode (GCE) (diameter 2.0 mm; Metrohm, Herisau, Switzerland) was used. pH values of the samples were measured with an 826 pH mobile digital pH meter (Metrohm).

Electroactive area (Ae) was determined to get more insight into the behavior of SiCO-based electrodic materials. Firstly, the effect of potential scan rate on the peak current of TBHQ and BHA at the SiCO materials and GCE was investigated in the range of 10-150 mV s^{-1}. For this assay, K$_4$[Fe(CN)$_6$] at 1.0×10^{-6} mol cm^{-3} was used as electrochemical probe employing 0.3 mol L^{-1} Britton-Robinson (BR) buffer as the supporting electrolyte. Therefore, the electroactive area was calculated using Randles-Sevcik, equation 6[28] from the slope of plot Ipa *vs.* v$^{1/2}$ (Figure S6, SI section).

$$Ipa = 2.69 \times 10^5 n^{3/2} AecD_0^{1/2} v^{1/2} \qquad (6)$$

where Ipa is the anodic peak current (A), n is the number of electrons in the redox reaction (n = 1), Ae is the electroactive area of the electrode (cm^2), c is the concentration of K$_4$[Fe(CN)$_6$] probe (1.0×10^{-6} mol cm^{-3}), D$_0$ is the diffusion coefficient of K$_4$[Fe(CN)$_6$] (7.6×10^{-6} cm^2 s^{-1}) and v is the scan rate (mV s^{-1}).

Results and Discussion

Preceramic polymers P1, P2 and P3

Three preceramic polymers containing different carbon contents were prepared from specific synthetic routes to evaluate the effect of organic fraction on ceramics structure, mainly regarding to evolution of SiC and C$_{free}$ phases.

Polycondensation reactions between reactive end silanol groups (Si−OH), from PDMF−OH silicone, and hydroxyl groups (−OH), from BPA organic crosslinker, took place with the aid of DDSn catalyst, giving rise to linear polymeric network P1 and water as by-product (Figure 1). The resulting polymeric structure, with higher carbon content, exhibits BPA molecules among linear silicone chains and its foam-like appearance might be justified by the schematic representation of bidimensional network and empty spaces owing to aromatic rings.
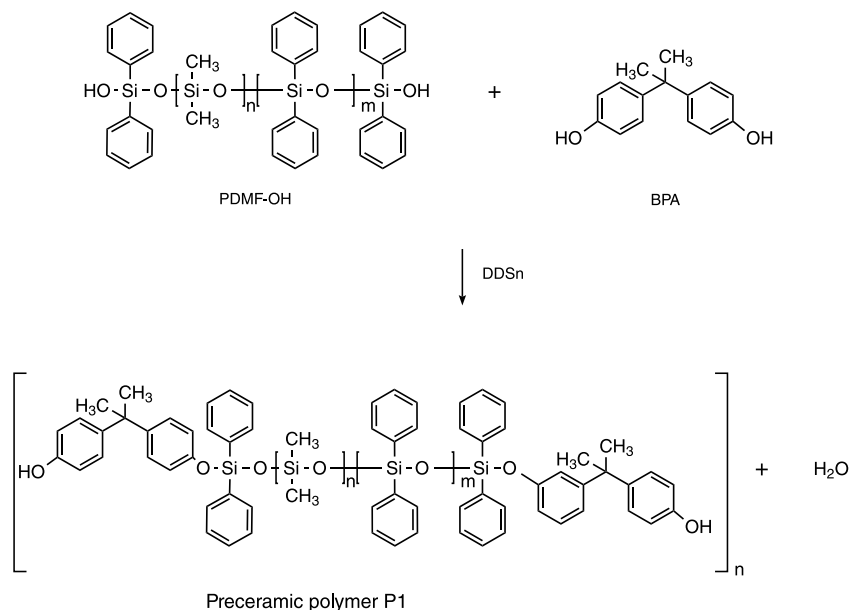
Figure 1. Schematic representation of the polymeric network P1, obtained by polycondensation reaction between linear PDMF–OH silicone and BPA organic crosslinker.

Polymeric network P2 was synthesized by radical reactions among cyclic D_4Vi chains, under heating and PDCM catalyst conditions, involving reactions among vinyl groups and, consequently, butylene bridges formation (Figure 2). Methyl groups may react with vinyl groups, forming propylene bridges, as well as reactions between two methyl groups may take place, generating ethylene bridges among cyclic silicone chains. However, the latter two reactions occur in lower extent, since the vinyl group presents greater reactivity and lesser steric hindrance regarding methyl group.[29] The most brittle aspect for P2 may be attributed to the polycyclic structural arrangement, providing a more opened tridimensional network in the absence of aromatic rings-containing groups.

Hydrosilylation reaction and schematic representation of molecular structure for P3 is shown in Figure 3, in which vinyl groups of DVB organic crosslinker react with Si–H bonds of PMHS silicone, forming ethylene bonds and no by-product. The most stiffness tridimensional polymeric network, containing intermediary carbon content, is composed of diethyl-phenylene bridges among silicone chains.

Structural and thermal characterization of the preceramic polymers

Polymerization reactions were investigated by comparing the FTIR spectra profiles of starting reagents with that obtained for resulting polymers, as can be seen in Figure S1 (SI section).

PDMF–OH, BPA and P1 (Figure S1a) exhibited common bands at 2970 and 1600 cm^{-1}, respectively assigned to $v(Csp^3–H)$ and $v(C=C)$.[30] PDMF–OH and P1 revealed absorption bands typical of dihydroxy terminated silicone, ascribed to $v(Si–CH_3)$, $v(Si–O–Si)$, $v(Si–C)$ and $\delta(Si–O)$ at 1250, 1033, 820 and 540 cm^{-1}, respectively, as well as $v(Si–Ph)$ and $\delta(Si–Ph)$ at 1450 and 702 cm^{-1} (+). For BPA, the main bands include $v(O–H)$, $v(C–O)$ (#) and $v(C–H)$ (#) at 3500, 1239 and 1203 cm^{-1}, together with *para*-substitution on aromatic ring at 848 cm^{-1} (*) and $\delta(O–H)$ out-of-plane bend (○).[30] The arising of a low intense band at 960 cm^{-1}, corresponding to $v(Si–O–Ph)$, combined with its foam-like appearance suggest the occurrence of polycondensation reactions between PDMF–OH and BPA, resulting in the preceramic polymer P1.[31] No vibrational mode corresponding to O–H bond was verified in the spectra for P1 and PDMF–OH, probably due to great difference of molar mass between polymer structure and end hydroxyl groups.

ATR FT-IR spectrum for D_4Vi (Figure S1b) exhibited typical bands for poly(organosiloxanes) attributed to $v(Si–CH_3)$, $v(Si–O–Si)$, $v(Si–C)$ and $\delta(Si–O)$, like in PDMF–OH, besides other bands at 3065, 2960, 1600, 1410, 960 and 745-791 cm^{-1}, ascribed to respective $v(Csp^2–H)$, $v(Csp^3–H)$, $v(C=C)$, $v(Si–CH=CH_2)$, $\delta(Si–CH=CH_2)$ (&) and $\delta(Si–CH_3)$.[31] The pronounced diminishing of bands ascribed to C=C and Si–CH=CH$_2$ bonds evidences the consumption of reactive vinyl groups during the radical polymerization reactions to obtain P2.

Absorption bands assigned to $v(Csp^3–H)$, $v(Si–CH_3)$, $v(Si–O–Si)$, $\delta(Si–CH_3)$ and $\delta(Si–O)$ were also verified for PMHS and P3 (Figure S1c),[32] in addition to $v(Si–H)$ and
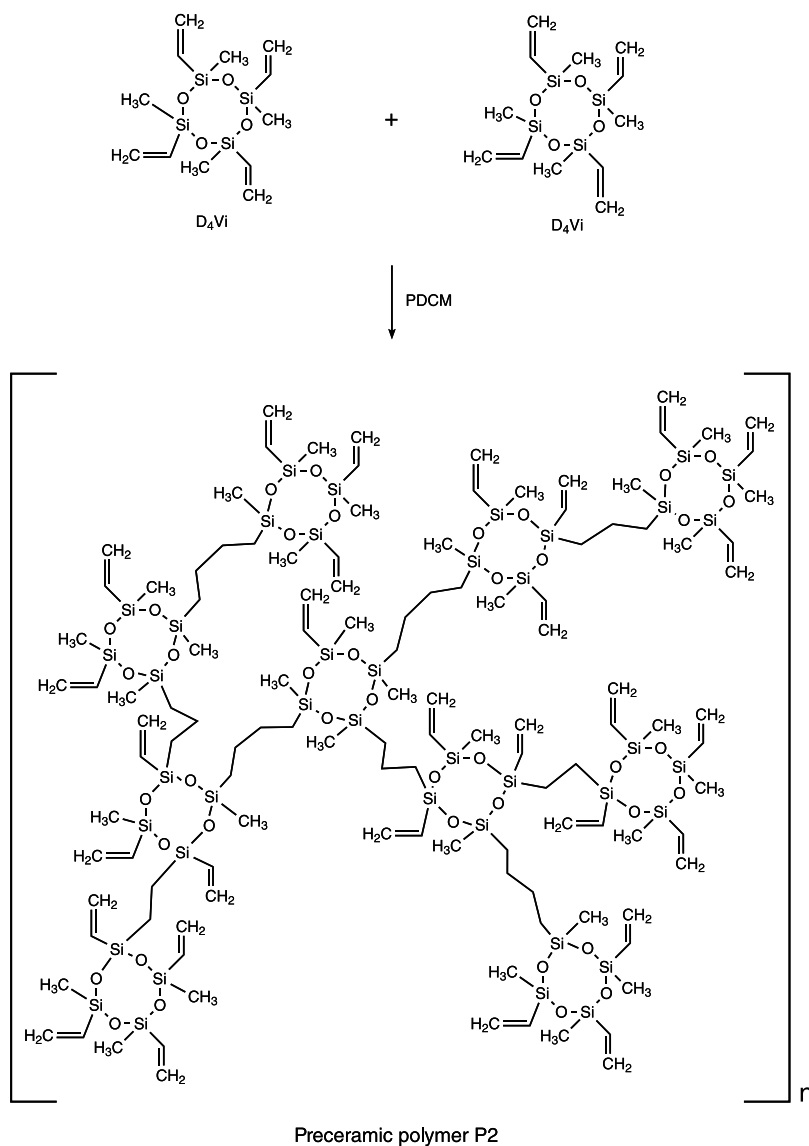
Figure 2. Schematic representation of the polymeric network P2, obtained by radical reaction among cyclic D$_4$Vi molecules.

δ(Si–H) at 2160 and 910 cm^{-1}, respectively.[3] For DVB, the main bands include υ(Csp^2–H) and υ(C=C) at 3088 and 1630 cm^{-1}.[30] Moreover, in the range of 1600-1300 cm^{-1}, bands corresponding to vibrational combination of C=C bonds present in the aromatic rings, besides at 990 cm^{-1} (%) and 850 cm^{-1} ($), respectively attributed to angular deformation out of plane and *para*-position of the aromatic ring, were observed.[30] Less intense bands corresponding to υ(Si–H) and υ(C=C), from respective reactive groups of silicone and organic crosslinker in P3 spectrum, associated to arising of a low intense band at 1178 cm^{-1}, assigned to Si–CH$_2$–CH$_2$–phenyl bonds,[31] suggest the occurrence of the hydrosilylation reaction.

Degradation processes in poly(organosiloxanes)-based polymeric networks usually involve breaking of CH$_3$ and CH$_2$–CH$_2$ bonds followed by the partial degradation of higher molar mass organic groups such as aromatic rings, when they are present, and the organic-inorganic transition.[33] The mineralization process from polymer to ceramic takes place with the breaking of Si–C, C–C and C–H bonds and releasing of volatile compounds, giving rise to ceramic network based on silicon oxycarbide.[33] Thermal degradation of preceramic polymers was evaluated by thermogravimetric analysis, according to TG and derivative thermogravimetry (DTG) curves, displayed in Figures 4a and 4b, respectively.

All preceramic polymers presented one thermal degradation event, according to DTG curves (Figure 4b), in which it was possible to determine the temperature values related to the beginning of decomposition process (T$_{onset}$) equal to 402, 479 and 457 °C, besides the maximum degradation rate (T$_{max}$) equal to 494, 502 and 507 °C, respectively for P1, P2 and P3.
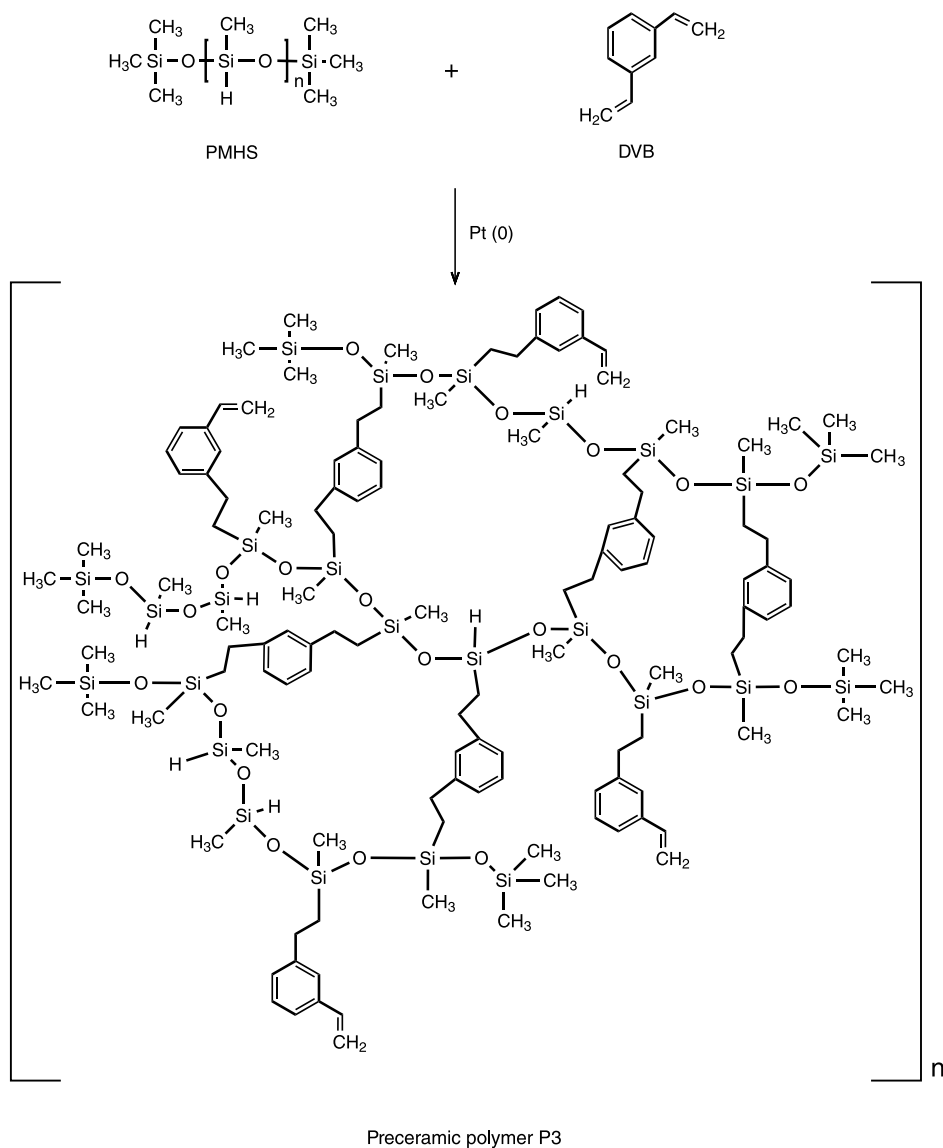
Preceramic polymer P3

Figure 3. Schematic representation of the polymeric network P3, obtained by hydrosilylation reaction between PMHS and DVB.
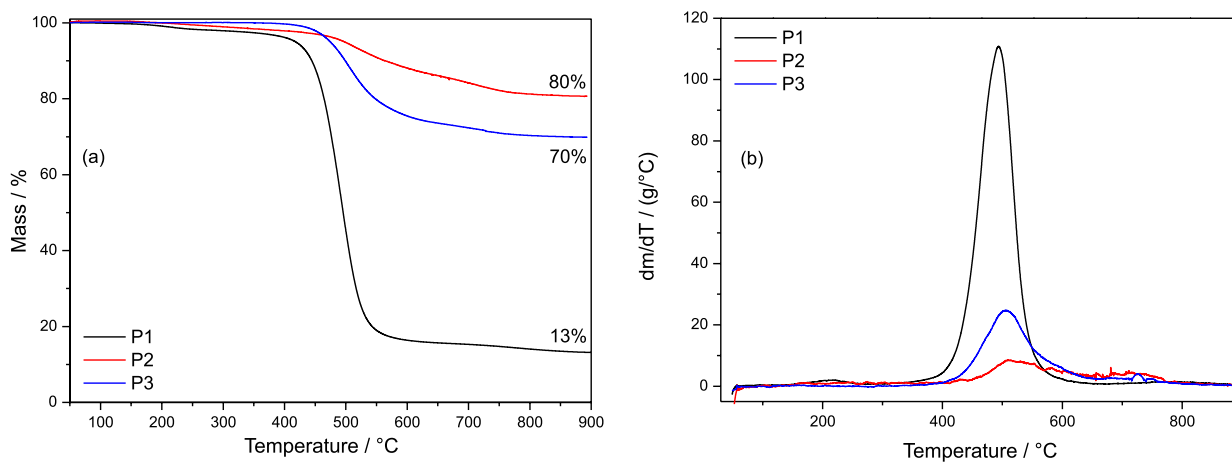

Figure 4. TG (a) and DTG (b) curves for preceramic polymers P1, P2 and P3.

P1 exhibited a less thermally stable polymeric network, followed by P3 and P1, according to corresponding T_{onset} values and displacement of TG curve to lower temperatures. Furthermore, the abrupt mass loss in a narrow temperature range for P1 (T_{max} at 494 °C) represents a typical degradation profile of linear polymer structures, whilst the gradual and continuous decomposition for P2 and P3 indicate a thermal decomposition behavior related to tridimensional polymeric networks, in agreement with the respective schematic representations (Figures 1-3).

Residual mass values were found to be 13, 80 and 70% for P1, P2 and P3, respectively (Figure 4a). The lowest value for P1 (13%) was associated to bidimensional polymeric network and higher carbon content owing to two starting reagents (PDMF–OH and BPA), as expected. Although both structures reveal tridimensional character, P3 showed lower ceramic yield (70%) than P2 (80%). This slightly difference might be justified by the presence of DVB fraction in P3 in comparison to polycyclic network P2, composed of purely inorganic bonds at main chain. Moreover, additional polymerization of residual Si-vinyl groups during heat treatment also contributed to the more interconnected polymeric network formation and the highest ceramic yield value for P2.[34]

Characterization of SiCO-based ceramics

Attenuated total reflection Fourier transform-infrared (FTIR-ATR) spectroscopy

C1, C2 and C3 were analyzed by FTIR-ATR spectroscopy to monitor structural transformations into ceramic matrices at two investigated pyrolysis temperatures. All samples revealed characteristic profiles of mineralized materials, evidenced by the absence of absorption bands corresponding to organic groups at polymers structure (Figure S2, SI section). The main bands at 1016, 794 and 443 cm^{-1}, respectively assigned to v(Si–O–Si), v(Si–C) and δ(Si–O), are typical of SiOC-based ceramic networks.[35] At 1000 °C, more intense bands attributed to v(Si–O–Si) when compared with v(Si–C) were noticed (Figure S2a). However, a contrary trend regarding such relative intensities for all samples was verified at 1500 °C due to more effective carbothermal reduction reaction (equation 2) at this temperature (Figure S2b). Furthermore, the displacement of bands to higher wavenumber values with respect to Si-containing bonds was attributed to the substitution of divalent oxygen by tetravalent carbon atoms, resulting in a more crosslinked ceramic network at higher temperatures, thus restricting its structural mobility.[36]

C2_1500 exhibited more intense band assigned to v(Si–C) when compared to the other samples. This suggests a better development of SiC phase, despite the absence of unsaturated organic groups at P2 structure (Figure 2) promotes lower residual carbon amounts after pyrolysis.

X-ray diffraction (XRD)

Different crystalline phases were investigated by XRD technique and the corresponding diffractograms for the ceramic materials at 1000 and 1500 °C are shown in Figure S3 (SI section).

All ceramics at 1000 °C exhibited a halo at 24° (2θ), referring to the amorphous phase composed of SiO$_4$, SiO$_3$C, SiO$_2$C$_2$, SiOC$_3$ and SiC sites randomly distributed in the matrix (Figure S3a).[5,32] Two diffraction signals at 43 and 50.5° (2θ), assigned to (100) and (004) planes of graphene sheets from disordered carbon phase, were verified, typical of C$_{graphitic}$.[37] These diffractions correspond to C$_{free}$ (or residual carbon) produced after incomplete decomposition of organic groups. The obtained values for the ratio between intensity (I$_p$) and full width at half maximum (FWHM) at 43° (2θ) peak (Ip/FWHM) were found to be 567.53 and 158.68 for C1_1000 and C3_1000, confirming that this phase was produced in higher proportion as the carbon content at preceramic polymer structure increased, as expected. The absence of this value for C2_1000 is justified by the extremely low diffraction signal at 43° (2θ), corroborating with the above affirmation. Peaks at 30.6, 31.9, 45.1, 55.4, 62.9 and 64.8° (2θ), ascribed to (200), (101), (211), (301), (112) and (321) crystallographic planes of tin,[19,38] were also observed for C1_1000 due to the presence of DDSn catalyst during the polymerization reaction. Furthermore, a well-defined peak at 74° (2θ), corresponding to (331) plane of silicon, was observed for all ceramics at 1000 °C.

Crystallization of ceramics at 1500 °C was evidenced by the presence of diffraction peaks at 35.5, 60 and 71.7° (2θ), attributed to the respective (111), (220), and (311) crystallographic planes of β-SiC phase,[39] effectively produced by carboreduction reaction at temperatures higher than 1200 °C (Figure S3b).[31] This process was accompanied by considerable diminishing of halo at 24° (2θ). C1_1500 revealed lower I$_p$/FWHM value (134.27) regarding to analogous sample at 1000 °C (567.53), considering the C(100) diffraction at 43° (2θ), due to the consumption of residual carbon to produce SiC via carboreduction (equation 2). Nevertheless, C3 samples revealed an opposite behavior, in which this ratio was 202.21 and 158.68 for C3_1500 and C3_1000, respectively. This result indicates that the C$_{graphitic}$ phase was predominantly produced in C3_1500 °C, once the low intense diffraction at 43° (2θ) made it impossible to accurately obtain such parameters for C2_1500. Aromatic groups-containing samples (C1_1500

and C3_1500) revealed sharper peak at 43° (2θ) when compared with C2_1500 (Figure S3b), as similarly verified for the set of samples at 1000 °C (Figure S3a). This result suggests that carbon was covalently bonded to silicone-based polymer structure through different polymerization reactions, giving rise to residual carbon into ceramics, whose proportions varied according to aromatic organic groups and polymer architecture.

For a better interpretation of the XRD patterns, Rietveld refinement method was employed to obtain the total percentage of crystalline SiC phase and amorphous fraction. The expected errors (R), obtained errors (R-WP) and R/R-WP ratios were found to be in the range 5.170-6.106%, 12.728-16.131% and 0.362-0.466, respectively, for all ceramic samples investigated. Table 1 exhibits total percentage values for both phases together with the average β-SiC crystallite sizes (t), estimated by Scherrer equation,[40] by considering the broadening line analysis on the diffraction peak at 35.5° (2θ).

Table 1. Total percentage values of crystalline SiC phase and amorphous fraction together with the average β-SiC crystallite sizes (t), estimated by Scherrer equation[31] from broadening line analysis on the diffraction peak at 35.5° (2θ), for ceramic materials obtained at 1000 and 1500 °C

Ceramic materials	Total percentage / %		t / nm
	SiC phase	Amorphous phase	
C1_1000	0.0	100.0	–
C2_1000	0.0	100.0	–
C3_1000	5.2	94.8	–
C1_1500	49.5	50.5	12.00
C2_1500	41.6	58.4	5.17
C3_1500	13.0	84.6	4.48

Crystallization process at 1500 °C was quantitatively confirmed by the appearance of SiC phase and diminishing of amorphous fraction for all ceramics. The highest value for SiC phase and its average crystallite size was found for C1_1500, followed by C2_1500 and C3_1500 (C1_1500 > C2_1500 > C3_1500). This trend was also confirmed by the Ip/FWHM values of 564.68, 219.19 and 108.71 for C1, C2 and C3 obtained at 1500 °C considering the most intense peak at 35.5° (2θ). The highest carbon amount at P1 precursor structure owing to both starting reagents contain aromatic groups (Figure 1) probably contributed to more effective formation of C_{free} into C1_1500, as already attested by the sharper peak at 43° (2θ). Carbon atoms in the neighboring of silicon atoms assist the formation of Si–C bonds,[41] becoming more favorable the carboreduction reaction (equation 2),[42] which justifies the highest percentage of SiC phase for C1_1500. Moreover,

the increase in the number of these bonds resulted in larger SiC crystallites.[43]

C2_1500 showed proportions of crystalline SiC phase and amorphous fraction close to C1_1500. Despite schematic representation of P2 structure suggests the lowest carbon amount (Figure 2), its polycyclic polymeric network makes be easier the devitrification process[23] to produce crystals in the resulting ceramic matrix. This behavior was earlier observed by the FTIR spectrum profile for C2_1500 (Figure S2b).

Crystalline SiC phase was produced in lower extent for C3_1500, resulting in the smallest crystallites (4.48 nm) and highest proportion of amorphous fraction regarding to the others. This might be related to the more thermally stable preceramic polymer, composed of a highly crosslinked tridimensional network, which hinders the devitrification during the carboreduction step towards SiC crystals evolution.[23]

Chemical composition

Empirical and stoichiometric formulae are compiled in Table 2 to illustrate chemical composition for all prepared materials. Carbon-richer polymers were obtained according to introduction of aromatic groups, by selecting starting materials and polymerization reaction, as stated by empirical formula for P1, P2 and P3.

Table 2. Empirical formula for preceramic polymers and ceramic materials, together with stoichiometric formula obtained for C1, C2 and C3 ceramics at 1000 and 1500 °C

Sample	Empirical formula	Stoichiometric formula
	$SiC_{(x+y)}O_{2(1-x)}H_w$	$SiC_xO_{2(1-x)} + yC_{free}$
P1	$SiC_{3.72}O_{1.21}H_{6.48}$	–
P2	$SiC_{2.31}O_{1.00}H_{4.69}$	–
P3	$SiC_{3.50}O_{1.82}H_{7.29}$	–
C1_1000	$SiC_{2.97}O_{1.65}H_{0.67}$	$SiC_{0.18}O_{1.65} + 2.79\,C_{free}$
C1_1500	$SiC_{2.24}O_{0.67}H_{0.08}$	$SiC_{0.66}O_{0.67} + 1.57\,C_{free}$
C2_1000	$SiC_{1.52}O_{1.56}H_{0.32}$	$SiC_{0.22}O_{1.56} + 1.30\,C_{free}$
C2_1500	$SiC_{0.98}O_{0.76}H_{0.07}$	$SiC_{0.62}O_{0.76} + 0.36\,C_{free}$
C3_1000	$SiC_{2.08}O_{1.66}H_{0.57}$	$SiC_{0.17}O_{1.66} + 1.91\,C_{free}$
C3_1500	$SiC_{1.55}O_{0.87}H_{0.02}$	$SiC_{0.57}O_{0.87} + 0.98\,C_{free}$

Pyrolyzed samples revealed lower carbon and hydrogen contents regarding to corresponding precursors, as expected, due to degradation process of polymeric network and continuous volatile compounds release such as hydrocarbons and hydrogen. The highest oxygen contents for ceramics at 1000 °C proved the mixed SiC_xO_{4-x} ($0 \leq x \leq 4$) network formation, mainly composed of Si–O rich sites.[44] Structural transformation and phases

segregation were evidenced for all ceramic samples through the lowest carbon, oxygen and hydrogen amounts with the temperature increasing. Besides redistribution reactions among the different silicon sites, carboreduction reactions effectively take place at temperatures ≥ 1200 °C,[33,42] mainly consuming Si–O and C species. The slightly difference among these elements confirms the balanced consumption of such species, as verified in the stoichiometric formulae.[36]

C_{free} phase was more effectively formed into carbon-richer ceramics, in the following order C1 > C3 > C2, attesting the influence of organic groups nature over residual carbon production. Both PDMF–OH silicone and BPA crosslinker containing aromatic groups for producing P1 (Figure 1) gave rise to a greater C_{free} amount into corresponding ceramic. The absence of aromatic groups at P2 structure (Figure 2) presented less contribution for producing of this carbonaceous phase. In this case, it was formed by degradation of saturated organic (methyl as well as ethylene, propylene and butylene bridges among D_4Vi chains) and residual vinyl groups. Intermediary values for C3 were compatible with the P3 composition and architecture, composed of aromatic groups only owing DVB crosslinker (Figure 3).

At 1500 °C, C_{free} diminished in relation to 1000 °C for all samples, due to carboreduction reaction, and this consumption was more pronounced for C1, confirming the SiC phase production in greater extent, as attested by the XRD.

Raman scattering spectroscopy

To gain deeper insights into the structural evolution of the carbon phase, Raman scattering spectroscopy was employed, according to spectra shown in Figure 5. All samples revealed the main bands typical of carbonaceous materials, comprising D and G bands, located around 1350

and 1580 cm^{-1}, respectively, as well as 2 D and D + G bands at 2500-3000 cm^{-1}.[24]

D band is a breathing mode of A_{1g} symmetry involving sp^2 carbon atoms in sixfold aromatic rings, whilst G band has E_{2g} symmetry and corresponds to in-plane bond stretching of all sp^2 carbon sites.[24] 2D band represents the overtone of D band and is always observed in defect-free samples at 2700 cm^{-1}.[45] Normally, these bands vary in intensity, position and width according to structural organization of the ceramics. Taking into account that C_{free} phase formed *in situ* in SiCO matrices after pyrolysis of poly(organosiloxanes) exhibits predominantly disordered nature,[19,41] its structural evolution might be interpreted according to stage 2 proposed by Ferrari and Robertson.[24] In this stage, the amorphization trajectory from nanocrystalline graphite to amorphous carbon (0% Csp[3] up to ca. 20% Csp[3]) is expressed by a schematic variation of the G position and I(D)/I(G) ratio, basically involving a decreasing of G band from 1600 to 1510 cm^{-1} and I(D)/I(G) → 0. Therefore, the development of D band indicates an ordering process in the disordered carbon phase, exactly the opposite trend for graphite, due to the increase of ordered rings' number.[24]

Table 3 illustrates D, G and 2D bands position, their respective widths at half height (W_D, W_G and W_{2D}), I_D/I_G and I_{2D}/I_G ratios, extracted after curve-fitting using the Lorentzian function, together with lateral average carbon-domains sizes (La), calculated according to equation 5.

Sharper and well-defined D and G bands were observed with increasing of the pyrolysis temperature, besides the displacement of G band to higher wavenumbers, indicating an enhanced organization of carbon phase accompanied by a decrease of carbon atoms with sp^3 hybridization.[24] This trend was also confirmed by the higher I_D/I_G values, suggesting an ordering process into C_{free} phase, which varies from amorphous carbon to nanocrystalline graphite, according to
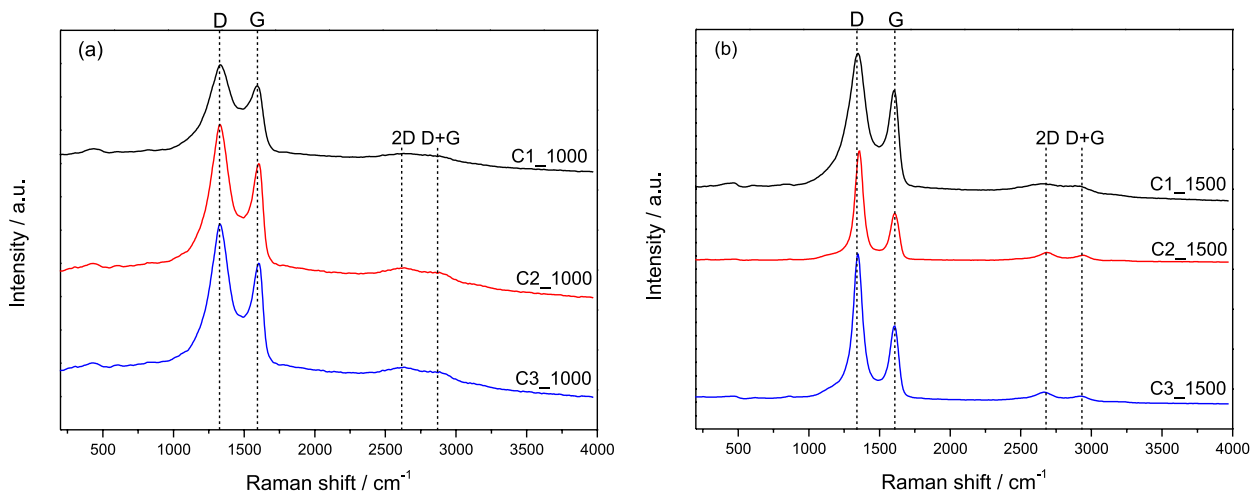

Figure 5. Raman spectra for C1, C2 and C3 ceramics obtained at 1000 °C (a) and 1500 °C (b).

Table 3. D, G and 2D bands position, width at half height of the respective bands (W_D, W_G and W_{2D}), I_D/I_G and I_{2D}/I_G ratios and lateral average carbon-domains sizes (La) for C1, C2 and C3 ceramics at 1000 and 1500 °C

Sample	D / cm^{-1}	G / cm^{-1}	2D / cm^{-1}	W_D / cm^{-1}	W_G / cm^{-1}	W_{2D} / cm^{-1}	I_D/I_G	I_{2D}/I_G	La / nm
C1_1000	1332	1600	–	205	72	–	1.75	–	1.68
C1_1500	1344	1608	2660	150	55	215	1.71	0.08	1.65
C2_1000	1328	1606	–	168	55	–	1.72	–	1.66
C2_1500	1347	1618	2684	75	42	130	3.57	0.15	2.40
C3_1000	1329	1606	–	169	54	–	1.73	–	1.67
C3_1500	1356	1626	2662	68	36	128	5.67	0.30	3.02

Ferrari and Robertson.[24] Furthermore, the arising of 2D band in samples at 1500 °C also proved the graphitization process containing more ordered and less defect carbon layers, resembling nanocrystalline graphite structure.[46] Overall, larger carbon domains were also obtained, mainly through transformations in the amorphous carbon fraction, once it is more susceptible to chemical reactions. The heat treatment favors structural transformations in the amorphous carbon phase, becoming it attached to the edges of the crystallite, thereby increasing their size.[47]

By comparing the C_{free} phase behavior produced from thermal degradation of the different preceramic polymers, C3_1500 exhibited G band at highest wavenumber (1626 cm^{-1}) and the lowest W_D and W_G values (68 and 36 cm^{-1}, respectively). This indicates the most effective graphitization process of the disordered carbon phase for P3 precursor derived SiCO ceramic. Furthermore, the highest I_D/I_G and I_{2D}/I_G values gave rise to larger carbon domains, confirming the greater evolution from amorphous carbon to nanocrystalline graphite structure for this ceramic.[24] This result might be justified by using PMS and DVB starting reagents that, according to Kleebe and Blum,[48] when they are submitted to pyrolysis procedure usually form a turbostratic carbon network due to the stacking of graphene layers and SiC nanocrystals generated by carboreduction. Hourlier *et al.*[46] investigated the *in situ* generation of nanographene domains in polymer-derived ceramic nanocomposites employing polyhydridomethylsiloxane (PHMS) and crosslinkers containing vinyl groups such as tetramethyl-tetravinylcyclotetrasiloxane (TMTVS) and divinylbenzene (DVB). They verified the formation of free Csp^2 domains into DVB-derived ceramic at lower temperatures that in the case of TMTVS crosslinker, being considered the first most structurally ordered carbon residue. The results evidenced that the DVB incorporation into silicone-based polymeric networks makes its thermal degradation hindered to generate volatile species, thereby turning into turbostratic carbon residues composed of few graphene layers embedded in the SiCO matrix. Most of the DVB retained in the resulting ceramic structure also might

justify the thermal degradation behavior of P3 precursor obtained in this study.

C2_1500 revealed better carbon phase organization than C1_1500, as demonstrated by the W_D, W_G, W_{2D}, I_D/I_G and I_{2D}/I_G parameters. This behavior is probably associated with the molecular architecture of the corresponding P2 and P1 preceramic polymers (Figures 1 and 2). Tridimensional character polycyclic network of P2 favors the organization process of the residual carbon phase, whilst the linear structure represented for P1 hinders the stacking of graphene layers produced during pyrolysis and, consequently, their evolution towards graphitization in the C_{free} phase.[46] Despite C1 ceramics exhibit the highest carbon amounts (Table 2), their more disordered nature made easier the reaction with Si–O domains to produce SiC, justifying the XRD patterns. Exactly following this trend are C2 and C3 ceramics that revealed a relationship between graphitization degree and production of semiconducting SiC phase.

Morphological investigation

Figure 6 exhibits SEM images of powdered preceramic polymers P1, P2 and P3, together with ceramic materials obtained at 1000 and 1500 °C. P1 revealed an exclusively smooth surface, typical of low-density materials.[49,50] Nevertheless, P2 and P3 presented similarities with each other, characterized by a rough and dense morphology, containing granular/globular particles at their surface, which possibly is associated to the tridimensional character of the respective polymeric networks (Figures 2 and 3) and, consequently, more stiffness materials.

In the overall, at 1000 °C, powdered ceramics exhibited a morphology composed of slate rock-like particles of various sizes and shapes.[51] SEM images at higher magnifications for C2_1000 and C3_1000 revealed a dense and pore free microstructure, typical of glasses matrices,[52] containing particles in lower amount but larger sizes with respect to those observed in the respective polymeric precursors. The dispersed particles seem to be melted due to the continuous heating treatment during the polymer-to-ceramic transition. Structures like entangled wires
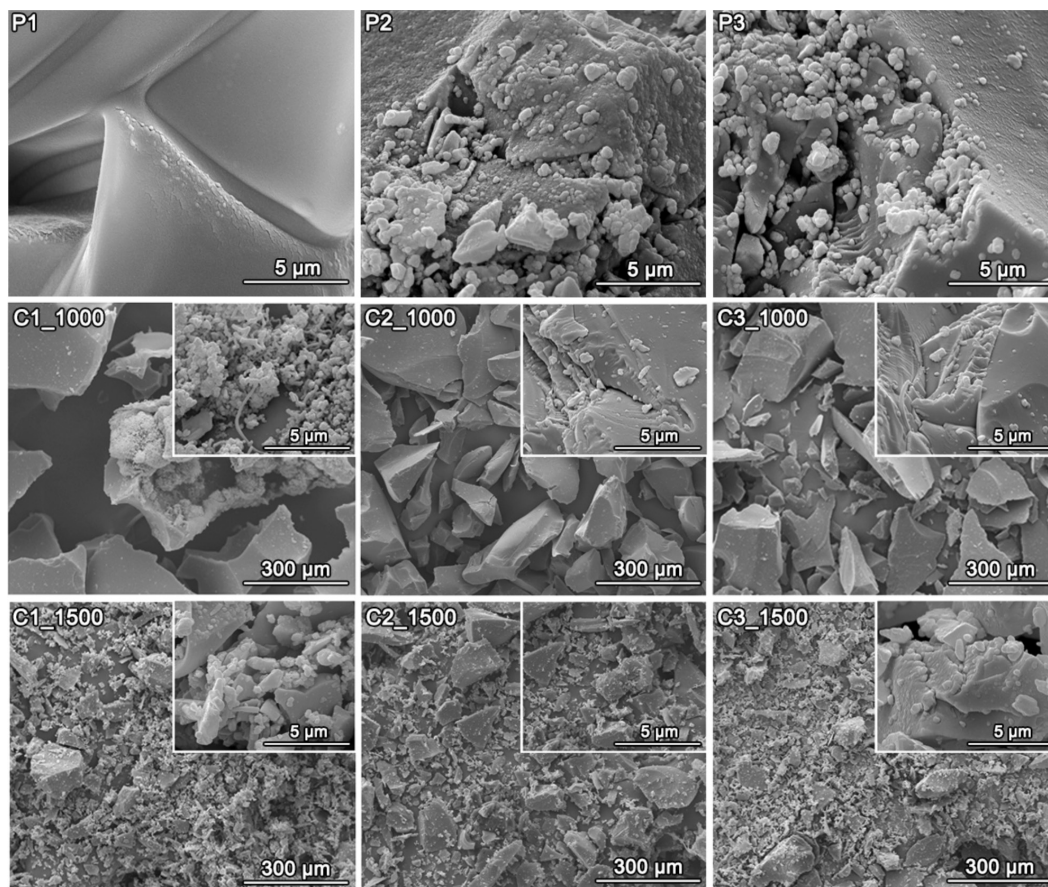
Figure 6. SEM images of preceramic polymers (P1, P2 and P3) and ceramic materials obtained at 1000 °C (C1_1000, C2_1000 and C3_1000) and 1500 °C (C1_1500, C2_1500 and C3_1500).

evolved at particles surface were observed in some regions of C1_1000 sample. The formation of such structures might be associated to pyrolysis process on carbon-richer precursor (P1). During the heating treatment, volatile organic compounds are more effectively released from P1 regarding P2 and P3, giving rise to reductive atmosphere inside alumina tube. The tin employed to obtain P1, in turn, may have catalyzed the production of these structures, in a similar condition to fabrication of carbon nanotubes by chemical vapor deposition (CVD) method.[53]

All ceramic samples at 1500 °C showed similar morphology, which was characterized by a rough morphology containing particles smaller than those observed in the materials obtained at 1000 °C. Moreover, joined particles were better observed at respective SEM images illustrated in the inset, evidencing the sintering and crystallization processes at higher temperatures.[54]

Evaluation of SiCO-based ceramics as electrodic materials for detection of TBHQ and BHA antioxidants

The electrochemical behavior of TBHQ and BHA at SiCO-based ceramics and GCE was evaluated by cyclic voltammetry under conditions previously studied of 0.03 mol L^{-1} BR buffer at pH 2.0. Voltammetric measures were initially performed over a wide pH range (2, 3, 4, 5, 6, 7, 8 and 9) using BR buffer solution. The results obtained at pH 2 revealed the highest anodic peak current (Ipa) values and better anodic peaks separation of phenolic compounds and, for this reason, this condition was used. Only C3_1500 electrode revealed electrochemical response, as clearly verified by the oxidation peaks for TBHQ and BHA (Figure 7). As displayed in Figure 6, this ceramic paste electrode exhibited higher anodic peak currents when compared with GCE. Additionally, the anodic peak potential for TBHQ was shifted towards less positive values, thus giving rise to a slight improvement in the anodic peak separation of compounds. Such outcome might be explained as result of phenolic compounds interaction at C3_1500 electrode surface as well as due to chemical nature of this ceramic material. The higher electroactive area for C3_1500 (0.0182 cm^2) compared to GCE (0.0065 cm^2) improves the interaction of phenolic compounds at the electrode-solution interface. The predominance of Csp^2 domains over Csp^3, i.e., more ordered residual carbon phase into ceramic matrix after pyrolysis, might also most

likely explain the better performance of C3_1500 electrode towards electrooxidation of phenolic compounds.
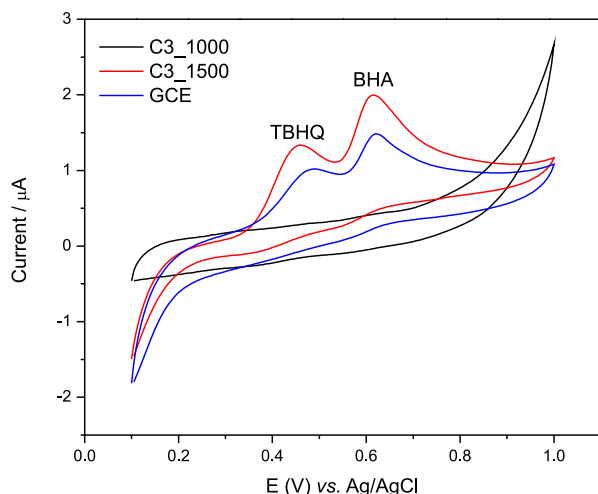

Figure 7. Cyclic voltammograms of TBHQ and BHA ethanol solution at 0.1 mmol L^{-1} concentration using C3_1000, C3_1500 and GCE in 0.3 mol L^{-1} BR buffer (pH 2.0) and scan rate of 50 mV s^{-1}.

All ceramic electrodes obtained at 1000 °C did not reveal measurable electrochemical response (Figures S4 (SI section) and Figure 7 for C3_1000). These results might be attributed to ceramic structure, predominantly composed of C$_{graphitic}$ domains and absence of crystalline SiC phase at this temperature (Figure S3a). Although C$_{graphitic}$ domains are present in the amorphous ceramic matrices, their particles are smaller and less organized than those embedded into analogous samples at 1500 °C (Table 3), hindering the charge transference at the electrode-solution interface.

In order to get a more insight into electrochemical performance of SiCO-based electrodes, static water contact angle experiments were carried out, as shown in Figure 8. As one can see, the respective contact angles for the C1_1500, C2_1500 and C3_1500 were found to be 122, 136 and 113°, thereby clearly indicating that C3_1500 exhibited higher hydrophilicity. The hydrophilic character might be associated to tetrahedral silicon sites (SiO$_4$, SiO$_3$C, SiC$_2$O$_2$, SiCO$_3$ and SiC$_4$) usually present into poly(organosiloxanes)-derived ceramic matrices. It is expected that SiCO materials richer Si–O give rise to more hydrophilic ceramic matrices, once this bonding has more ionic character with respect to Si–C and C–C bonds, allowing better interaction with polar molecules of solvent. Furthermore, each oxygen atom remains with two free electron pairs, contributing to enhance the hydrophilicity of ceramic and, consequently, the solvation process with solvent molecules.

The presence of acidic sites in the ceramics together with the static contact angle data might greatly contribute to a better understanding of phenolic compounds interaction at the electrode-solution interface. The acidic sites were determined through Boehm titration method,[27] originally developed for studying the acidic properties of activated carbons, as well as employed to evaluate acidic and basic groups on SiC.[55] In the SiCO-based matrices, acidic sites comprise rich Si–O domains, mainly the SiO$_4$, considered the most acidic site when compared with the others. Therefore, the reaction of SiCO materials with NaOH solution (strong base) and further titration with HCl solution is a simple experimental procedure to estimate the proportion of acidic sites in the ceramic matrices. C1_1500, C2_1500 and C3_1500 revealed acidic sites concentration of 20, 60 and 100 mmol g^{-1}, respectively. The highest hydrophilicity for C3_1500, as observed in Figure 8, might be associated to the highest acidic sites concentration. This result, combined with the ceramic structure, favors the interaction between electrode and the phenolic compounds and further electrooxidation at electrode-solution interface.[56,57] Although C1_1500 has showed hydrophilicity somewhat similar to the C3_1500 (Figure 8), the first one showed the lowest acidic sites concentration, which is probably related to its more crystalline profile (Figure S3 and Table 1) and higher residual carbon (C$_{free}$) content (Table 2). The high hydrophilicity of C1_1500 might also be attributed to the physical features of material, which in turn, greatly influences in handling paste into the cavities of electrode. The thermal treatment at 1500 °C of linear P1 precursor resulted in a finely powder ceramic, thus contributing to the easiest handling paste. According to results, it seems that the less ordered carbon phase in C1_1500 and C2_1500, whose development is related to the polymer chemistry
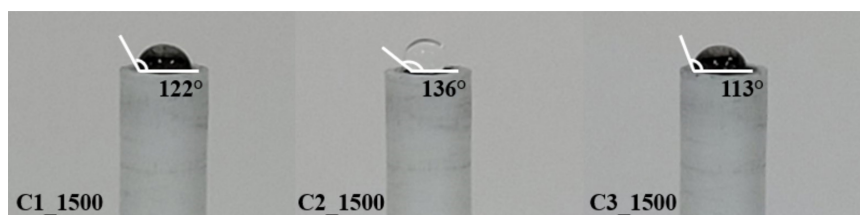

Figure 8. Profiles of water drop at surface of C1_1500, C2_1500 and C3_1500 materials prepared in an 80:20 wt.% ratio (ceramic:Nujol®), compacted into a cavity electrode followed by polishing with paper flat surface and washing with ultrapure water.

(carbon content and architecture), played a great influence to justify the absence of electrochemical response for these ceramics.

Conclusions

Silicon oxycarbide (SiCO) ceramics with varied carbon contents were obtained by controlled pyrolysis route of three preceramic polymers in the presence and absence of aromatic carbon groups and evaluated as electrodic materials in voltammetric measurements for detection of TBHQ and BHA antioxidants. Production and phases development on ceramic materials were influenced according to molecular architecture and chemical composition of precursors together with pyrolysis temperature.

SiCO materials at 1000 °C basically exhibited amorphous nature containing $C_{graphitic}$ domains embedded into ceramic matrices, whose proportions increased as the carbon amount at precursor structure increased. Crystallization process in all samples obtained at 1500 °C was evidenced through the evolution of SiC phase with simultaneous consumption of residual carbon phase. SiC phase was more effectively produced in C-richer SiCO ceramics, which revealed more disordered C_{free} phase, demonstrating a relationship between graphitization degree and SiC production.

Ceramic sample obtained at 1500 °C from preceramic polymer with intermediary carbon content (C3_1500) revealed good electrochemical performance in terms of peak current and peak separation for simultaneous TBHQ and BHA determination, while the other ceramics cannot be used as electrodic materials in voltammetric measures. These results have been associated to ceramic structure, mainly regarding to evolution of graphitization process and acidic sites concentration. While the first brings information about Csp^2 and Csp^3 sites, the second one is assigned to hydrophilicity of ceramic structure. In summary, C3_1500 showed great potentialities to be used as a new electrodic material for simultaneous determination of TBHQ and BHA antioxidants with over advantages to commercial glassy carbon electrode.

Supplementary Information

Supplementary data are available free of charge at http://jbcs.sbq.org.br as PDF file.

Acknowledgments

References

1. Colombo, P.; Mera, G.; Riedel, R.; Sorarù, G. D.; *J. Am. Ceram. Soc.* **2010**, *93*, 1805. [Crossref]

2. Tahir, M. S.; Weinberger, M.; Balasubramanian, P.; Diemant, T.; Behm, R. J.; Lindén, M.; Wohlfahrt-Mehrens, M.; *J. Mater. Chem. A* **2017**, *5*, 10190. [Crossref]

3. Godoy, N. V.; Pereira, J. L.; Duarte, E. H.; Tarley, C. R. T.; Segatelli, M. G.; *Mater. Chem. Phys.* **2016**, *175*, 33. [Crossref]

4. Arango-Ospina, M.; Xie, F.; Gonzalo-Juan, I.; Riedel, R.; Ionescu, E.; Boccaccini, A. R.; *Appl. Mater. Today* **2020**, *18*, 100482. [Crossref]

5. Mazo, M. A.; Tamayo, A.; Rubio, J.; *J. Eur. Ceram. Soc.* **2016**, *36*, 2443. [Crossref]

6. Pan, J.; Shen, W.; Zhao, Y.; Sun, H.; Guo, T.; Cheng, Y.; Zhao, N.; Tang, H.; Yan, X.; *Colloids Surf., A* **2020**, *584*, 124041. [Crossref]

7. Iastrenski, M. F.; da Silva, P. R. C.; Tarley, C. R. T.; Segatelli, M. G.; *Ceram. Int.* **2019**, *45*, 21698. [Crossref]

8. Pan, J.; Pan, J.; Cheng, X.; Yan, X.; Lu, Q.; Zhang, C.; *J. Eur. Ceram. Soc.* **2014**, *34*, 249. [Crossref]

9. Sorarù, G. D.; Modena, S.; Guadagnino, E.; Colombo, P.; Egan, J.; Pantano, C.; *J. Am. Ceram. Soc.* **2004**, *85*, 1529. [Crossref]

10. de Almeida, M.; Romagnoli, S.; de Carvalho, R.; Tarley, R. T.; Gava, M.; *Mater. Chem. Phys.* **2020**, *254*, 123503. [Crossref]

11. Xia, K.; Liu, X.; Liu, H.; Lu, Y.; Liu, Z.; Li, Y.; Duan, L.; Hou, Z.; Li, R.; Wang, D.; *Electrochim. Acta* **2021**, *372*, 137899. [Crossref]

12. Greenough, M.; Zhao, Z.; Jacobsohn, L. G.; Tong, J.; Bordia, R. K.; *J. Eur. Ceram. Soc.* **2021**, *41*, 5882. [Crossref]

13. Deriabin, K. V.; Yaremenko, I. A.; Chislov, M. V.; Fleury, F.; Terent'Ev, A. O.; Islamova, R. M.; *New J. Chem.* **2018**, *42*, 15006. [Crossref]

14. Pan, J.; Ren, J.; Xie, Y.; Wei, X.; Guan, Y.; Yan, X.; Tang, H.; Cheng, X.; *Res. Chem. Intermed.* **2017**, *43*, 3813. [Crossref]

15. Troegel, D.; Stohrer, J.; *Coord. Chem. Rev.* **2011**, *255*, 1440. [Crossref]

16. Cordelair, J.; Greil, P.; *J. Eur. Ceram. Soc.* **2000**, *20*, 1947. [Crossref]

17. Zhao, P.; Hao, J.; *Food Chem.* **2013**, *139*, 1001. [Crossref]

18. Angelis, P. N.; Mendonça, J. C.; Rocha, L. R.; Capelari, T. B.; Prete, C.; Segatelli, M. G.; Borsato, D.; *Electroanalysis* **2020**, *32*, 1198. [Crossref]

19. Segatelli, M. G.; Coelho, G. R.; Romagnoli, É. S.; Catarini da Silva, P. R.; *Ceram. Int.* **2021**, *47*, 6030. [Crossref]

20. Segatelli, M. G.; Radovanovic, E.; Gonçalves, M. C.; Yoshida, I. V. P.; *J. Eur. Ceram. Soc.* **2009**, *29*, 3279. [Crossref]

21. Lim, D. J.; Marks, N. A.; Rowles, M. R.; *Carbon N. Y.* **2020**, *162*, 475. [Crossref]

22. Dibandjo, P.; Graczyk-Zajac, M.; Riedel, R.; Pradeep, V. S.; Soraru, G. D.; *J. Eur. Ceram. Soc.* **2012**, *32*, 2495. [Crossref]

23. Dibandjo, P.; Diré, S.; Babonneau, F.; Soraru, G. D.; *J. Non.-Cryst. Solids* **2010**, *356*, 132. [Crossref]

24. Ferrari, A. C.; Robertson, J.; *Phys. Rev. B* **2000**, *61*, 14095. [Crossref]

25. Suquila, F. A. C.; de Oliveira, L. L. G.; Tarley, C. R. T.; *Chem. Eng. J.* **2018**, *350*, 714. [Crossref]

26. Rasband, W. S.; *ImageJ*, version 1.53; U. S. National Institutes of Health, Bethesda, Maryland, USA, 2021.

27. Boehm, H. P.; *Carbon N. Y.* **1994**, *32*, 759. [Crossref]

28. Bard, A. J.; Faulkner, L. R.; Swain, E.; Robey, C.; *Fundamentals and Applications*; John Wiley: New York, US, 2000.

29. McMurry, J.; *Quimica Orgânica*; Thomson: Stamford, US, 2008.

30. Coates, J. In *Encyclopedia of Analytical Chemistry: Applications, Theory and Instrumentation*; John Wiley: New York, US, 2006. [Crossref]

31. Launer, P. J.; Arkles, B.; *Silicon Compounds: Silanes and Silicones*; Gelest Inc.: Morrisville, PA, USA, 2013, p. 175.

32. Wang, L.; Lu, K.; Ma, R.; *Appl. Phys. A: Mater. Sci. Process.* **2019**, *125*, 395. [Crossref]

33. Schiavon, M. A.; Ferrari, J. L.; Hojamberdiev, M.; Yoshida, I. V. P.; *Quim. Nova* **2015**, *38*, 972. [Crossref]

34. Ambadas, G.; Packirisamy, S.; Ninan, K. N.; *J. Mater. Sci. Lett.* **2002**, *21*, 1003. [Crossref]

35. Nyczyk-Malinowska, A.; Wójcik-Bania, M.; Gumuła, T.; Hasik, M.; Cypryk, M.; Olejniczak, Z.; *J. Eur. Ceram. Soc.* **2014**, *34*, 889. [Crossref]

36. Mazo, M. A.; Tamayo, A.; Rubio, F.; Soriano, D.; Rubio, J.; *J. Non.-Cryst. Solids* **2014**, *391*, 23. [Crossref]

37. Suboch, A. N.; Cherepanova, S. V.; Kibis, L. S.; Svintsitskiy, D. A.; Stonkus, O. A.; Boronin, A. I.; Chesnokov, V. V.; Romanenko, A. I.; Ismagilov, Z. R.; Podyacheva, O. Y.; *Fullerenes, Nanotubes, Carbon Nanostruct.* **2016**, *24*, 520. [Crossref]

38. Wu, J.; Zhu, Z.; Zhang, H.; Fu, H.; Li, H.; Wang, A.; Zhang, H.; Hu, Z.; *J. Alloys Compd.* **2014**, *596*, 86. [Crossref]

39. Lu, K.; Erb, D.; *Int. Mater. Rev.* **2018**, *63*, 139. [Crossref]

40. Cullity, B. D.; Stock, S. R.; *Elements of X-Ray Diffraction*; Prentice Hall: New Jersey, 2001.

41. Segatelli, M. G.; Sanchez, P. M.; Silva, L. R. C.; Silva, M. A.; Tarley, C. R. T.; da Silva, P. R. C.; Ribeiro, E. S.; *J. Braz. Chem. Soc.* **2021**, *32*, 1222. [Crossref]

42. Stabler, C.; Ionescu, E.; Gonzalo-juan, I.; Graczyk-zajac, M.; Riedel, R.; *J. Am. Ceram. Soc.* **2018**, *101*, 4817. [Crossref]

43. Brequel, H.; Parmentier, J.; Sorar, G. D.; Schiffini, L.; Enzo, S.; *Nanostruct. Mater.* **1999**, *11*, 721. [Crossref]

44. Xu, T.; Ma, Q.; Chen, Z.; *Mater. Lett.* **2011**, *65*, 433. [Crossref]

45. Mera, G.; Navrotsky, A.; Sen, S.; Kleebe, H.-J.; Riedel, R.; *J. Mater. Chem. A* **2013**, *1*, 3826. [Crossref]

46. Hourlier, D.; Venkatachalam, S.; Ammar, M. R.; Blum, Y.; *J. Anal. Appl. Pyrolysis* **2017**, *123*, 296. [Crossref]

47. Gangadhar, J.; Maheshwari, A.; Bordia, R. K.; Shyam Kumar, C. N.; Kubel, C.; Sujith, R.; *Ceram. Int.* **2020**, *46*, 28156. [Crossref]

48. Kleebe, H. J.; Blum, Y. D.; *J. Eur. Ceram. Soc.* **2008**, *28*, 1037. [Crossref]

49. Deville, S.; *Adv. Eng. Mater.* **2008**, *10*, 155. [Crossref]

50. Yu, Z.; Feng, Y.; Li, S.; Pei, Y.; *J. Eur. Ceram. Soc.* **2016**, *36*, 3627. [Crossrer]

51. Knozowski, D.; Vallachira Warriam Sasikumar, P.; Madajski, P.; Blugan, G.; Gazda, M.; Kovalska, N.; Wilamowska-Zawłocka, M.; *Nanomaterials* **2022**, *12*, 410. [Crossref]

52. Segatelli, M. G.; Radovanovic, E.; Pires, A. T. N.; Gonalves, M. D. C.; Yoshida, I. V. P.; *Mater. Chem. Phys.* **2010**, *124*, 1216. [Crossref]

53. Usoltseva, A.; Kuznetsov, V.; Rudina, N.; Moroz, E.; Haluska, M.; Roth, S.; *Phys. Status Solidi B* **2007**, *244*, 3920. [Crossref]

54. Duan, L.; Ma, Q.; Chen, Z.; *J. Eur. Ceram. Soc.* **2013**, *33*, 841. [Crossref]

55. Kim, M. S.; Rhee, K. Y.; Park, S.-J.; *Composites, Part B* **2016**, *94*, 218. [Crossref]

56. Alulema-Pullupaxi, P.; Fernández, L.; Debut, A.; Santacruz, C. P.; Villacis, W.; Fierro, C.; Espinoza-Montero, P. J.; *Chemosphere* **2021**, *278*, 130488. [Crossref]

57. Du, Y.; Gan, Y.; Yang, P.; Cuie, Z.; Hua, N.; *Mater. Chem. Phys.* **2007**, *103*, 446. [Crossref]